JPn Neuroscience

The Journal of Physiology

J Physiol 594.13 (2016) pp 3827–3840

Altered development in GABA co-release shapes glycinergic synaptic currents in cultured spinal slices of the SOD1^{G93A} mouse model of amyotrophic lateral sclerosis

Manuela Medelin[1], Vladimir Rancic[1], Giada Cellot[1], Jummi Laishram[1], Priyadharishini Veeraraghavan[2], Chiara Rossi[3], Luca Muzio[3], Lucia Sivilotti[4] and Laura Ballerini[1,2]

[1] *Department of Life Sciences, University of Trieste, Trieste, Italy*
[2] *International School for Advanced Studies (SISSA/ISAS), Trieste, Italy*
[3] *Neuroimmunology Unit, Division of Neuroscience, Institute of Experimental Neurology (INSPE), San Raffaele Scientific Institute, Milan, Italy*
[4] *Department of Neuroscience, Physiology and Pharmacology, University College London (UCL), London, UK*

Key points

- Increased environmental risk factors in conjunction with genetic susceptibility have been proposed with respect to the remarkable variations in mortality in amyotrophic lateral sclerosis (ALS).
- *In vitro* models allow the investigation of the genetically modified counter-regulator of motoneuron toxicity and may help in addressing ALS therapy.
- Spinal organotypic slice cultures from a mutant form of human superoxide dismutase 1 (SOD1G93A) mouse model of ALS allow the detection of altered glycinergic inhibition in spinal microcircuits.
- This altered inhibition improved spinal cord excitability, affecting motor outputs in early SOD1^{G93A} pathogenesis.

Abstract Amyotrophic lateral sclerosis (ALS) is a fatal, adult-onset neurological disease characterized by a progressive degeneration of motoneurons (MNs). In a previous study, we developed organotypic spinal cultures from an ALS mouse model expressing a mutant form of human superoxide dismutase 1 (SOD1^{G93A}). We reported the presence of a significant synaptic rearrangement expressed by these embryonic cultured networks, which may lead to the altered development of spinal synaptic signalling, which is potentially linked to the adult disease phenotype. Recent studies on the same ALS mouse model reported a selective loss of glycinergic innervation in cultured MNs, suggestive of a contribution of synaptic inhibition to MN dysfunction and degeneration. In the present study, we further exploit organotypic cultures from wild-type and SOD1^{G93A} mice to investigate the development of glycine-receptor-mediated synaptic currents recorded from the interneurons of the premotor ventral circuits. We performed single cell electrophysiology, immunocytochemistry and confocal microscopy and suggest that GABA co-release may speed the decay of glycine responses altering both temporal precision and signal integration in SOD1^{G93A} developing networks at the postsynaptic site. Our hypothesis is supported by the finding of an increased MN bursting activity in immature SOD1^{G93A} spinal cords and by immunofluorescence microscopy detection of a longer persistence of GABA in SOD1^{G93A} glycinergic terminals in cultured and *ex vivo* spinal slices.

(Resubmitted 4 March 2016; accepted after revision 7 April 2016; first published online 21 April 2016)
Corresponding author L. Ballerini: International School for Advanced Studies (SISSA/ISAS), via Bonomea 265 I-34136 Trieste, Italy. Email: laura.ballerini@sissa.it

DOI: 10.1113/JP272382

Abbreviations ALS, amyotrophic lateral sclerosis; CNQX, 6-cyano-7-nitroquinoxaline-2,3-dione; GAD65, glutamic acid decarboxylase 65; GlyT2, glycine transporter 2; mPSCs, miniature glycinergic currents; MNs, motoneurons; gly-PSCs, glycine-receptor mediated synaptic currents; PBS, phosphate-buffered saline; PSC, post synaptic current; RT, room temperature; $SOD1^{G93A}$, mutant form of human superoxide dismutase 1; VR, ventral root; WIV, weeks *in vitro*; WT, wild-type.

Introduction

Familial and sporadic forms of amyotrophic lateral sclerosis (ALS) are characterized by a progressive degeneration of upper and lower motoneurons (MNs) (Ling *et al.* 2013). Many diverse disease mechanisms have been proposed (Rothstein, 2009), focusing most recently on specific alterations in protein- and/or ribonucleic-metabolic pathways (Robberecht & Philips, 2013), which is a hypothesis supported by genetic analysis, including exome sequencing in sporadic ALS (Cirulli *et al.* 2015). Nevertheless, it is still unclear how different molecular pathologies determine two important features of ALS: the great variability in the time of disease onset and the selective vulnerability of MNs, with variable patterns across MN pools in the spinal cord (Robberecht & Philips, 2013).

Approximately 20% of familial ALS cases are associated with mutations in the superoxide dismutase 1 (SOD1 OMIM*147450) gene. Transgenic mice expressing additional copies of the human mutant gene are good models of adult-onset ALS (McGoldrick *et al.* 2013). These display neurodegenerative processes mimicking human ALS and are the most widely used models for investigating the molecular pathways correlated with disease onset (Rothstein, 2003; Turner & Talbot, 2008). A strong case can be made for investigating ALS and other neurodegenerative processes in immature neuronal networks, aiming to capture pre-symptomatic alterations in synaptic signalling (Ben-Ari, 2008). It was recently reported that spinal synaptic inhibition is insufficient in mice expressing a mutated human SOD1, $SOD1^{G93A}$ (Chang & Martin, 2009, 2011; Martin & Chang, 2012). Cultured $SOD1^{G93A}$ MNs display a selective loss of glycinergic innervation compared to age-matched wild-type (WT) MN (Chang & Martin, 2011). Using organotypic cultures from mouse spinal cords to model network development (Avossa *et al.* 2003; Rosato-Siri *et al.* 2004; Furlan *et al.* 2007), we reported, in mutant $SOD1^{G93A}$, an imbalance between synaptic excitation and inhibition, as well as increased MN susceptibility to mild excitotoxic stressors *in vitro* (Avossa *et al.* 2006). However, it is unknown how the spatiotemporal expression of the glycinergic/GABAergic system and its contribution to early pre-motor network function is affected during spinal maturation in $SOD1^{G93A}$ mice.

In the present study, we further exploit organotypic cultures from WT and $SOD1^{G93A}$ mice to investigate glycine-receptor mediated postsynaptic currents (gly-PSCs). We found that the speeding up of the decay phase of gly-PSCs with spinal maturation was greater in $SOD1^{G93A}$ interneurons compared to WT, despite the broadly similar properties of glycinergic single channel activity in age-matched WT and $SOD1^{G93A}$ patches. The most probable explanation for the difference in gly-PSC decay may be that $SOD1^{G93A}$ synapses retain greater GABA co-expression and co-release than WT, a hypothesis supported by our observation of the effects of depleting glycinergic terminals of GABA, as well as by immunofluorescence microscopy detection of GABA in glycinergic terminals. The influence of the greater GABA co-localization on spinal integrated motor outputs was examined using isolated WT and $SOD1^{G93A}$ neonatal spinal cords via multiple ventral root (VR) recordings. In developing $SOD1^{G93A}$ spinal cords, spontaneous bursting events in VR recordings were found to be longer compared to WT. When this activity was recorded in the presence of a $GABA_A$ receptor antagonist, we also detected, in $SOD1^{G93A}$ spinal networks, an enhanced excitation characterized by faster bursting. Thus, more persistent GABA co-release may affect temporal precision and signal integration in $SOD1^{G93A}$ developing networks at the postsynaptic site.

Methods

Preparation of spinal tissue cultures and isolated spinal cords

Transgenic mice ($SOD1^{G93A}$) expressing a high copy number of the glycine 93 to alanine mutation of the hSOD1 gene (B6SJL-TgN(SOD1-G93A)1Gur) (Gurney *et al.* 1994) and non-transgenic females (B6SJLF1) were purchased from Jackson Laboratories (Bar Harbor, ME, USA) and bred as reported previously (Avossa *et al.* 2006). The WT $SOD1^{G93A}$ littermates were used as negative controls for the genetic background (Holasek *et al.* 2005; Schutz, 2005; Copray *et al.* 2003; Rao *et al.* 2003). Genotyping was determined by PCR analysis as reported previously (Avossa *et al.* 2006). Briefly, organotypic slice cultures of spinal cord and dorsal root ganglia were obtained from mouse embryos at days 12–13 of

gestation as described previously (Avossa *et al.* 2003, 2006; Rosato-Siri *et al.* 2004; Furlan *et al.* 2005, 2007). Experiments were performed on WT and SOD1^{G93A} sister cultures at 1, 2 and 3 weeks *in vitro* (WIV).

For the preparation of acute WT and SOD1^{G93A} spinal slices, mice were killed at P0 by cervical dislocation and spinal cords were collected in ice-cold phosphate-buffered saline (PBS) as described previously (Nigro *et al.* 2012), then fixed in 4% formaldehyde (prepared from fresh paraformaldehyde; Sigma, St Louis, MO, USA) in PBS, pH 7.2 for 6 h at 4°C. Spinal cords were cryoprotected in PBS-30% sucrose (Sigma) and then embedded in optical cutting temperature (Bio-Optica, Milan, Italy) inclusion media. Samples were stored at –80°C before sectioning at 12 μm.

For VR recordings, the entire spinal cords were isolated from WT and SOD1^{G93A} neonatal mice (P2–P4) as reported previously (Bracci *et al.* 1996; Beato & Nistri, 1999; Taccola *et al.* 2008; Veeraraghavan & Nistri 2015). Briefly, animals were decapitated, internal organs were removed and a laminectomy was performed to expose and remove the spinal cord. Preparations were continuously superfused with standard Krebs solution containing (in mM): 113 NaCl, 4.5 KCl, 1 $MgCl_2 \cdot 7H_2O$, 2 $CaCl_2$, 1 NaH_2PO_4, 25 $NaHCO_3$ and 11 glucose, gassed with 95% O_2 and 5% CO_2 (pH 7.4) at room temperature (RT).

Genotyping was performed after the electrophysiological experiments had been performed to allow the electrophysiological experimenter to be 'blind' to animal genotype. PCR analysis was then performed as reported previously (Avossa *et al.* 2006).

Ethical statement

All experiments were performed in accordance with the EU guidelines (2010/63/UE) and Italian law (decree 26/14) and were approved by the local authority veterinary service and by our institution (SISSA-ISAS) ethical committee. All efforts were made to minimize animal suffering and to reduce the number of animal used. Animals use was approved by the Italian Ministry of Health, in agreement with the EU Recommendation 2007/526/CE.

Electrophysiological recordings

For patch clamp recordings (whole-cell, voltage clamp mode), a coverslip with the spinal culture was positioned in a recording chamber, mounted on an inverted microscope and superfused with control physiological saline solution containing (in mM): 152 NaCl, 4 KCl, 1 $MgCl_2$, 2 $CaCl_2$, 10 Hepes and 10 glucose. The pH was adjusted to 7.4 with NaOH (osmolarity 305 mosmol l^{-1}). Cells were patched with pipettes (4–7 MΩ) filled with a solution of the composition (in mM): 120 K gluconate, 20 KCl, 10 HEPES, 10 EGTA, 2 $MgCl_2$ and 2 Na_2ATP. The pH was adjusted to 7.3 with KOH (295 mosmol l^{-1}). All electrophysiological recordings were performed at RT.

The reported voltage values are corrected for the liquid junction potential (−14 mV) if not otherwise indicated. The series resistance value was <10 MΩ enabling recordings of synaptic currents without significant distortion, and thus was not compensated for (Streit *et al.* 1991; Furlan *et al.* 2007). Recordings were performed from ventrally located spinal interneurones identified on the basis of previously reported criteria (Ballerini & Galante, 1998; Ballerini *et al.* 1999; Galante *et al.* 2000). Electrophysiological responses were amplified (EPC-7, HEKA; Multiclamp 700B; Axon Instruments, Foster City, CA, USA), sampled and digitized at 10 kHz with pCLAMP software (Axon Instruments) for offline analysis. Single spontaneous synaptic events were detected using AxoGraph X (Axograph Scientific, Berkeley, CA, USA) event detection software (Clements & Bekkers, 1997) and Clampfit, version 10 (pClamp suite; Axon Instruments). On average, ≥400 events were analysed from each cell to obtain mean kinetic and amplitude parameters. From the average of these events, we measured the rise time, defined as the 10–90% time needed to reach the peak of the synaptic current, the peak amplitude and the decay time constant (expressed as τ) by fitting a mono-exponential function.

We detected no differences between WT ($n = 56$) and SOD1^{G93A} ($n = 52$) interneurones in membrane capacitance (64 ± 6 pF WT, 63 ± 5 pF SOD1^{G93A}) and input membrane resistance (231 ± 32 MΩ WT, 228 ± 22 MΩ SOD1^{G93A}). Gly-PSCs were recorded at a holding potential of −84 mV in the presence of 6-cyano-7-nitroquinoxaline-2,3-dione (CNQX) (10 μM; Sigma) and SR-95531 (10 μM; Sigma). To detect glycinergic mPSCs, TTX (1 μM; Latoxan, Valence, France) was added. Gly-PSCs and mPSCs were abolished by the application of 1 μM strychnine (Sigma).

TBOA (30 μM; Tocris Bioscience, St Louis, MO, USA) was added to the perfusion for ≥10 min to deplete GABA presynaptic vesicular content.

For outside-out recordings, the standard physiological saline solution used was the same as that the in whole-cell recordings; the pipette solution contained (in mM): 140 CsCl, 4 NaCl, 1 $MgCl_2$, 0.5 $CaCl_2$, 5 EGTA, 10 Hepes and 2 MgATP. The pH was adjusted at 7.3 (290 mosmol l^{-1}).

Outside-out patches were obtained in the presence of TTX (1 μM), CNQX and SR-95531 (both 10 μM) in the extracellular medium and 5 μM QX-314 in the intracellular solution and held at –84 mV. We recorded for 40 s in control solution to ensure that the patch did not display any baseline channel openings before applying glycine (15 μM) through the perfusion system. This glycine concentration was considered to be the most suitable for evoking substantial receptor activation and for avoiding any excessive multichannel activity that would be difficult

to analyse. Under these conditions, we observed five simultaneous channel openings at most at the beginning of the glycine application. After 1 min of equilibration in glycine solution, traces were analysed for at least 30 s or for as long as the quality of the recording was sufficient to allow us to measure the amplitude of openings clearly. Between 15 and 30 channel openings were measured in each trace. In noisy patches, only clear openings were considered.

Homomeric glycine receptors are known to have higher conductance than heteromers. In conditions similar to the those employed in the present study (e.g. high symmetrical chloride), homomeric conductance is greater than 86 pS and heteromeric conductance is 45–54 pS, regardless the α subunit type (Bormann *et al.* 1993).

We classified the patches into three groups, depending on the type of channel openings that they contained: (i) heteromeric GlyR patches, where all openings were between 4 and 5 pA (corresponding to a chord conductance of 47–59 pS); (ii) homomeric GlyR patches, where all openings were between 7 and 8 pA (83–95 pS); or (iii) mixed GlyR patches where both 4–5 pA and 7–8 pA openings was detected, suggesting the presence of a mixed population of homomeric and heteromeric receptors.

The main risk in the analysis would be to classify two simultaneous heteromeric openings as a single homomeric opening. We examined the trace at appropriate sweep speed to check whether a transition was a double event or not. If the transition appeared to be a single opening to the larger conductance, we validated the classification by checking that it was followed by a closure of the same amplitude.

Furthermore, this error is improbable, given that the amplitude of homomeric openings is less than twice that of heteromeric ones: the average current amplitudes were 7.6 ± 0.3 and 4.3 ± 0.2 pA for homomeric and heteromeric openings, respectively ($n = 13$ patches). In traces with homomeric channels openings, we occasionally observed openings to a lower conductance (2.9 ± 0.1 pA, $n = 11$ patches). These openings were much smaller than heteromeric openings and may represent sublevels of the homomeric conductance, as reported previously (Bormann *et al.*, 1993).

For the study of motor output from the isolated spinal cord, VRs of the lumbar region segments (L2 and L5) were tightly inserted, by applying a gentle negative pressure, in monopolar suction electrodes connected to Ag/Ag-Cl micropellets in glass micropipettes. Spontaneous activity was also recorded in the presence of the GABA receptor antagonist SR-95531 (10 μM) to investigate the network activity controlled by glycinergic transmission as an inhibitory source. At least 10 min of recordings was used to analyse burst periodicity. Signals were amplified (DP-304 differential amplifier; Molecular Devices, Sunnyvale, CA, USA), digitized at 20 kHz and recorded with pCLAMP software (Molecular Devices) for offline analysis.

Immunofluorescence

WT and SOD1^{G93A} cultures were fixed with 4% formaldehyde (prepared from fresh paraformaldehyde) in PBS for 60 min at RT and then washed in PBS. Free aldehyde groups were quenched in 0.1 M glycine in PBS for 5 min. The samples were blocked and permeabilized in 3% fetal bovine serum, 3% BSA and 0.3% Triton-X 100 in PBS for 30 min at 37°C. Samples were incubated with primary antibodies (guinea-pig anti-glycine transporter 2, GlyT2, Millipore, Billerica, MA, USA, dilution 1:1000; rabbit anti-glutamic acid decarboxylase 65, GAD65, Santa Cruz Biotechnology, Santa Cruz, CA, USA, dilution 1:50) diluted in PBS with 5% fetal bovine serum at 4°C, overnight. Samples were then incubated in secondary antibodies (Alexa 488 goat anti-guinea-pig, Invitrogen, Carlsbad, CA, USA, dilution 1:400; Alexa 594 goat anti-rabbit, Invitrogen, dilution 1:400; DAPI, Invitrogen, final concentration 5 μg ml^{-1}) for 2 h at 37°C and finally mounted on glass coverslips using Vectashield hardset mounting medium (Vector Laboratories, Inc., Burlingame, CA, USA). For acute spinal cord slices, the same staining protocol was used, with the exception of the blocking step where a solution of 10% horse serum and 0.3% Triton-X 100 in PBS was used to enhance the penetration of the antibodies into the tissue.

Images were acquired using a C2 Confocal Microscope (Nikon, Tokyo, Japan) equipped with Ar/Kr, He/Ne and UV lasers. Images were acquired with a 40× oil-objective (numerical aperture 1.3) using oil-mounting medium (1.515 refractive index). Confocal sections were acquired every 0.5 μm up to a total sample thickness of 12 μm. Regions of interest were confined to the ventral part of slice. Offline analysis of the image *z*-stack was performed using NIS-Elements AR software (Nikon) and the open source image-processing package FIJI (http://fiji.sc/Fiji).

To investigate the amount of GlyT2 and GAD65 co-localization in WT and SOD1^{G93A}, we used the image analysis software Volocity (PerkinElmer, Waltham, MA, USA). In both channels, a threshold was set for both the intensity and the object size, thus ensuring that the observed signal indicates the presence of genuine GlyT2 and GAD65 signals. We quantified only those voxels that represented co-localized GlyT2 signals with GAD65 signals.

Statistical analysis

The results are presented as the mean ± SE, if not otherwise indicated; n is the number of neurons. A statistically significant difference between two data sets was assessed by Student's t test (after checking variances homogeneity by Levene's test) for parametric data and by Mann–Whitney's test for non-parametric ones. $P < 0.05$ was considered at a statistically significant.

A chi-squared test was used to assess the statistically significant differences in outside-out experiments.

Results

Glycinergic synaptic currents in developing WT and SOD1^{G93A} spinal interneurons

We recorded spontaneous gly-PSCs in isolation by patch clamping ventral interneurons from WT and SOD1^{G93A} spinal cord slices in the presence of CNQX and SR-95531 to block PSCs mediated by AMPA/kainate and $GABA_A$ receptors (Fig. 1*A* and *B*). Organotypic spinal networks mature during *in vitro* culture (Avossa *et al.* 2003; Furlan *et al.* 2007). This was reflected in WT cultures by a progressive increase in the frequency and peak amplitude of spontaneous gly-PSCs recorded at 1, 2 and 3 WIV (Fig. 1*A*, *C* and *D*). These developmental changes were similar in age-matched SOD1^{G93A} cultures (Figure 1*B*–*D*). WT and SOD1^{G93A} interneurons displayed similar values of gly-PSC frequency and amplitude in the developmental window analysed. Thus, the mean frequency values increased from 3.3 ± 0.7 Hz at 1 WIV to 11.1 ± 0.9 Hz at 3 WIV and from 1.8 ± 0.5 Hz at 1 WIV to 11.6 ± 1.7 Hz at 3 WIV for WT and SOD1^{G93A} cultures, respectively (Fig. 1*C*). The mean peak amplitude values increased from 25.0 ± 6.7 pA at 1 WIV to 41.0 ± 4.1 pA at 3 WIV and from 18.6 ± 5.3 pA to 45.7 ± 6.6 pA for WT and SOD1^{G93A} cultures, respectively (Fig. 1*D*).

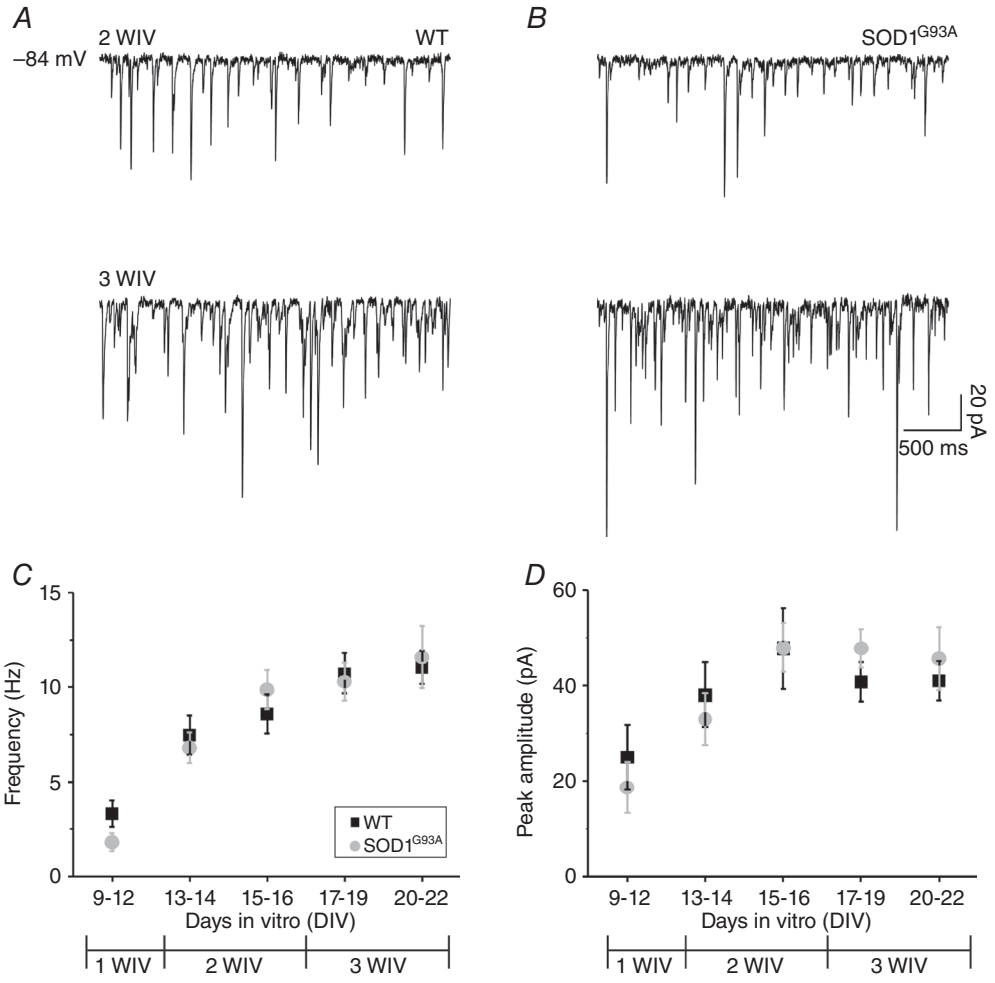

Figure 1. WT and SOD1^{G93A} ventral interneurons display similar developmental regulation in gly-PSC frequency and amplitude
Representative traces of spontaneous gly-PSCs recorded at 2 WIV (top) and 3 WIV (bottom) in (*A*) WT and (*B*) aged-matched SOD1^{G93A}. Plots of gly-PSC frequency (*C*) and amplitude (*D*) values for WT (black) and SOD1^{G93A} (grey) interneurons; note the changes brought about by *in vitro* maturation (total number of neurons was 93 WT and 76 SOD1^{G93A}, with ≥400 PSCs analysed per cell; divided by DIV: 9–12 DIV, 4 WT and 5 SOD1^{G93A}; 13–14 DIV, 6 WT and 10 SOD1^{G93A}; 15–16 DIV, 12 WT and 10 SOD1^{G93A}; 17–19 DIV, 33 WT and 31 SOD1^{G93A}; 20–22 DIV, 38 WT and 20 SOD1^{G93A}).

In the next set of measurements, because of the relatively low frequency of glycinergic events at 1 WIV, we focused on older ages (2 and 3 WIV) to compare the development of the kinetic properties of spontaneous gly-PSCs in WT and SOD1^{G93A} slices. It is well established that the decay of GlyR-mediated currents speeds up during physiological synaptic development because of a switch from the expression of α2 GlyR subunits (probably forming homomeric GlyRs) to that of the classical adult synaptic GlyR, an $\alpha1\beta$ heteromer (Malosio *et al.* 1991; Takahashi *et al.* 1992; Singer *et al.* 1998; Aguayo *et al.* 2004; Beato & Sivilotti, 2007; Lynch, 2009). The traces in Fig. 2*A* show that this process occurs also in our explants, and that the decay time constant (τ) of gly-PSCs in both WT and SOD1^{G93A} interneurons becomes progressively shorter with *in vitro* maturation. Thus, the τ value of WT gly-PSCs progressively shifted from 14.6 ± 1.9 ms at the beginning of the 2 WIV to 7.6 ± 0.3 ms at the end of the 3 WIV; similarly,

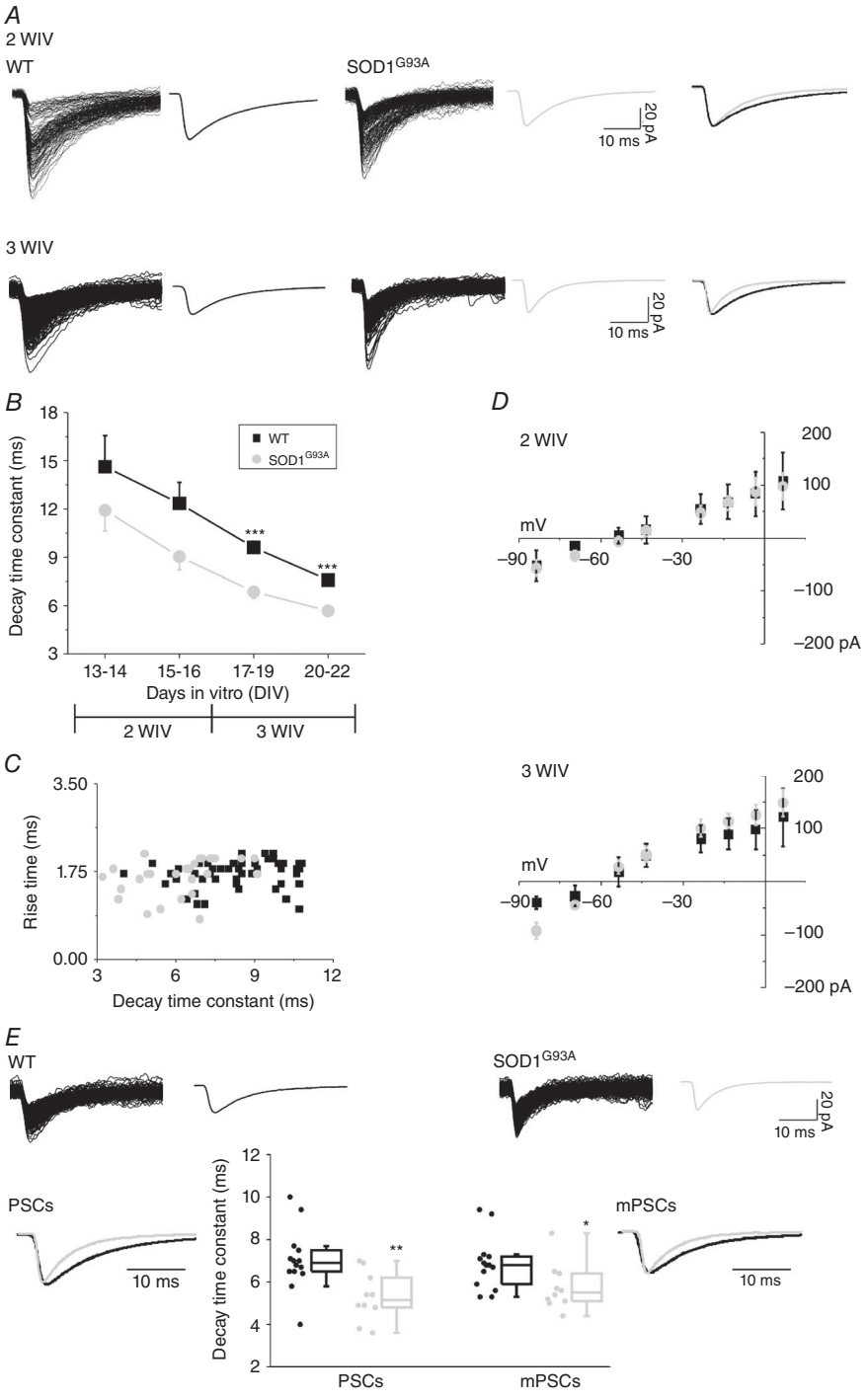

Figure 2. SOD1^{G93A} gly-PSCs decay faster than WT gly-PSC after *in vitro* development
A, superimposed traces show pharmacologically isolated gly-PSCs recorded from WT (left) and SOD1^{G93A} (middle) ventral interneurones at 2 WIV (top row) and 3 WIV (bottom row; average PSCs to the side). The traces to the right are WT (black) and SOD1^{G93A} (grey) average traces superimposed and scaled to the peak to highlight the different decay time. *B*, plot of the changes in the decay time constant (τ) during *in vitro* growth (overall 74 WT and 52 SOD1^{G93A}; divided by DIV: 13–14 DIV, 6 WT and 10 SOD1^{G93A}; 15–16 DIV, 12 WT and 10 SOD1^{G93A}; 17–19 DIV, 26 WT and 16 SOD1^{G93A}; 20–22 DIV, 30 WT and 16 SOD1^{G93A}). *C*, scatter plot of rise time *vs.* decay time; in both WT and SOD1^{G93A} at 3 WIV (56 WT and 32 SOD1^{G93A}) regression analysis reveals no linear relationship between these two parameters ($r = 0.2344$, probability = 0.095 and $r = 0.3435$, probability = 0.093 for WT and SOD1^{G93A} neurons, respectively). *D*, *I–V* curves were obtained by plotting gly-PSCs mean amplitude against Vh at 2 WIV (top) and 3 WIV (bottom) for WT and SOD1^{G93A} ventral interneurons (31 WT and 23 SOD1^{G93A}). Note that the approximate calculated reversal potential was –55 mV at 2 WIV and –60 mV at 3 WIV. *E*, superimposed individual WT and SOD1^{G93A} gly-mPSCs and average mPSCs (top row). The estimated average gly-PSC and mPSC charges (area under the curve) were: WT 459.7 ± 83.4 pA × ms and 170.2 ± 19.5 Pa × ms, PSCs and mPSCs, respectively; SOD1^{G93A} 294.9 ± 33.2 pA × ms and 139.5 ± 15.2 pA × ms, PSCs and mPSCs, respectively. Bottom row: box plots of the decay time constants of WT and SOD1^{G93A} glycinergic PSCs and mPSCs (14 WT and 10 SOD1^{G93A}); superimposed average and scaled tracings are gly-PSCs (left) and gly-mPSCs (right) for WT (black) and SOD1^{G93A} (grey). *$P < 0.05$; **$P < 0.01$; ***$P < 0.001$.

the decay of SOD1^{G93A} gly-PSCs (11.9 ± 1.3 ms at 2 WIV) became faster at 3WIV (5.7 ± 0.3 ms) (Fig. 2*A* and *B*). In SOD1^{G93A} interneurones, gly-PSC appeared to decay faster than WT at 2 WIV, a difference that became highly significant as the variability across neurons decreased at 3 WIV (Fig. 2*B*) ($P = 0.000001$). The absence of correlation between PSC rise time *vs.* decay time values (Fig. 2*C*) suggests that that differences in recording conditions, location of synapses or electronic filtering probably did not affect our observations.

Figure 2*D* shows the measurement of the reversal potential of gly-PSCs in WT and SOD1^{G93A} at 2WIV (Fig. 2*D*, top) and at 3 WIV (Fig. 2*D*, bottom). The approximate theoretical value expected for the Cl^- equilibrium potential for our intracellular and extracellular chloride concentrations is –50 mV. At 2 and 3 WIV, the measured reversal potentials were more negative (by 5 mV and 10 mV, at 2 and 3 WIV) than the calculated one (Fig. 2*D*). However, the reversal potential values and their shifts were identical in WT and SOD1^{G93A} neurons, suggesting that local intracellular chloride concentrations are similar.

The higher gly-PSC frequency in explants after 3 WIV allowed us to extend our characterization to the properties of mPSCs (recorded in the presence of TTX). The results in this group of cells (Fig. 2*E*) confirm that WT and SOD1^{G93A} mPSCs differ in their decay kinetics (mPSCs τ value: 6.9 ± 0.3 ms WT and 5.8 ± 0.3 ms SOD1^{G93A}; $P = 0.035$) in a manner similar to that of spontaneous gly-PSCs recorded before TTX treatment (gly-PSCs τ value: 7.0 ± 0.4 ms WT and 5.3 ± 0.4 ms SOD1^{G93A}).

The faster decay in glycinergic synaptic currents recorded in SOD1^{G93A} interneurons could be the result of a difference in the GlyRs that mediates these synaptic events. To test this hypothesis, in an independent set of experiments, we performed outside-out recordings from 2 and 3 WIV interneurons. Figure 3*A* shows typical examples of such recordings, where the channel opening are downwards. Although the density of channels openings was too high to allow us to measure the burst length of these channels (and compare it with the PSC decay τ), it was easy to measure the amplitude of the openings, and therefore the channel conductance. For glycine channels, conductance is a straightforward indication of the homomeric or heteromeric nature of the receptor because it is higher for homomers (greater than 86 pS in high symmetrical chloride) than for heteromers (45–54 pS) (Bormann *et al.* 1993), irrespective of the α subunit involved. The top trace in Fig. 3*A* is from a patch (2 WIV) where the predominant channel amplitude was between 4 and 5 pA (see horizontal dashed lines). This current amplitude corresponds to a conductance of 58 pS, which would suggest that the activity arises from heteromeric receptors. The bottom trace shows another patch, where the most common openings were large (7–8 pA) and therefore probably stem from homomeric receptors. The middle trace shows a recording where channels with small (4–5 pA) and large (7–8 pA) amplitudes coexist, indicating the presence of a mixed population of homomeric and heteromeric receptors.

Thus, patches were categorized in three populations depending on the conductances detected: ∼50 pS, ∼90 pS or mixed. The prevalence of the different types at different ages *in vitro* is depicted in Fig. 3*B*. Intriguingly, at 2 WIV, in WT slices, 77% of patches displayed the smaller conductance, indicating a more mature GlyR expression (Takahashi *et al.* 1992), whereas, in transgenic cultures, 56% of the patches still showed mostly high conductance channel activity or a mixed population of low and high conductance channels, suggesting a delay in GlyRs maturation. This delayed maturation implies the persistence of the homomeric channels in transgenic cultures that, if anything, should make gly-PSCs slower than WT in their decay. By contrast, gly-PSCs at 2 WIV appeared faster in their decay (not significant) in SOD1^{G93A} explants (Fig. 2*B*). At 3 WIV, the prevalence of the different conductance patterns was similar for patches from WT and SOD1^{G93A}. This rules out the possibility that the difference in decay at 3 WIV was a result of large differences in the GlyRs populations expressed by the two groups (Fig. 3*A* and *B*).

GABA co-release tunes glycine PSCs τ in SOD1^{G93A} spinal interneurons

During antenatal development, one-third of the neurons located in the ventral spinal cord co-express glycine and GABA (Allain *et al.* 2006; Sibilla & Ballerini, 2009); thus, we tested the ability of this amino acid to shape gly-PSCs, by glycine displacement from GlyRs, when co-released (Lu *et al.* 2008). We hypothesized that the faster gly-PSCs τ in SOD1^{G93A} could be the result of a delay in the maturation of glycine-GABA mixed synapses and, ultimately, the persistence of GABA co-release. GABA pre-synaptic content was depleted by TBOA (WT and SOD1^{G93A}) (Mathews and Diamond, 2003), a broad-spectrum competitive antagonist of glutamate transporters (Shimamoto *et al.* 1998) that inhibits the glutamate uptake needed for GABA synthesis. Figure 3*C* and *D* shows that, at 3 WIV, TBOA treatment did not affect WT gly-PSCs decay (τ values: 8.4 ± 0.9 ms and 9.1 ± 1.0 ms before and after the perfusion with TBOA, respectively) but slowed down SOD1^{G93A} gly-PSCs decay (τ values: 5.7 ± 0.5 ms and 7.4 ± 0.8 ms before and after the addition of TBOA, respectively). The difference in decay time between the two genotypes is statistically significant before the application of TBOA ($P = 0.008$), whereas, after treatment, the decay values become comparable ($P = 0.22$). Our hypothesis was further supported by immunostaining experiments where we targeted GlyT2

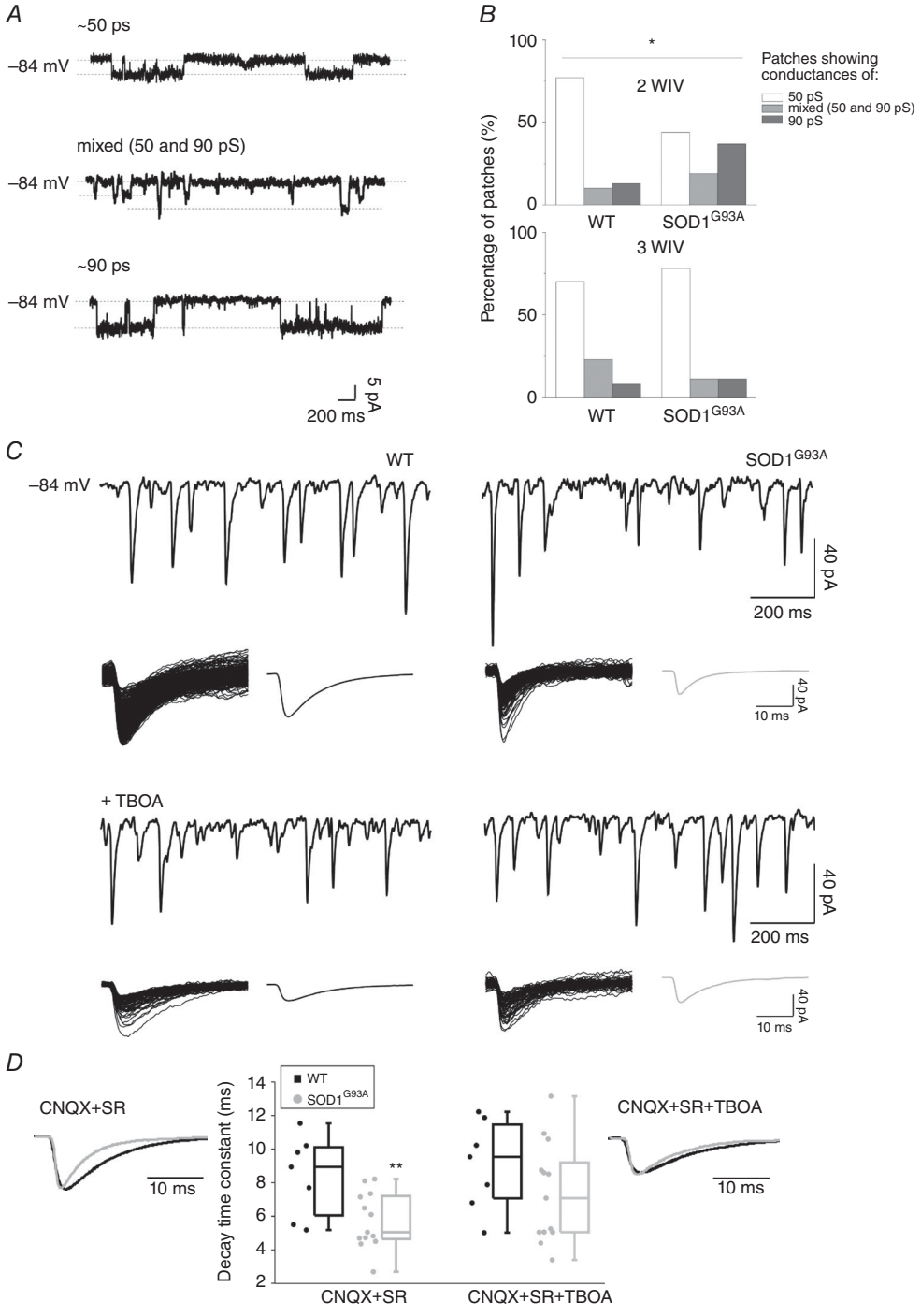

Figure 3. GlyR-mediated single-channel activity in outside-out WT and SOD1^{G93A} patches and contribution of GABA co-release in shaping spontaneous gly-PSCs in WT and SOD1^{G93A} synapses
A, representative current traces from outside-out patches with low or high conductances (top and bottom, respectively) and for a patch with a mixed population of conductances (middle). Dashed lines represent diverse amplitude of channel opening for different receptor types. Channel openings were elicited by bath application of glycine (15 μM) at a Vh of −84 mV. *B*, proportion of patches in the three conductance categories (~50 pS, mixed, ~90 pS) at 2 ($n = 82$) and 3 WIV ($n = 23$) in WT and SOD1^{G93A}. *C*, representative traces of spontaneous WT (left) and SOD1^{G93A} (right) gly-PSCs before (top row) and after (bottom row) TBOA (30 μM) application. The superimposed glycinergic events and their average trace (to the right) are depicted below each recording. *D*, box plot summary of the WT and SOD1^{G93A} mean decay time constant values for gly-PSCs before and after TBOA application (7 WT and 13 SOD1^{G93A}); WT (black) and SOD1^{G93A} (grey) gly-PSCs averaged traces are scaled and superimposed in the absence (left) and in the presence (right) of TBOA. $^{*}P < 0.05$; $^{**}P < 0.01$.

and GAD65 to quantify the presynaptic co-localization and to detect mixed glycine-GABA terminals (Dumoulin *et al.* 2001; Mackie *et al.* 2003; Dugué *et al.* 2005). At 3 WIV, co-localization of GlyT2-GAD65 is more common in transgenic cultures than in WT, and this supports our electrophysiological results (Fig. 4*C* and *E*). Notably, a very similar result was obtained when we repeated the measurement in acute slices isolated from the spinal cord of WT and SOD1^{G93A} neonatal (P0) mice. GABA-glycine co-localization is more prevalent in the transgenic tissue (Fig. 4*A*, *B* and *D*), further supporting our electrophysiological results and validating organotypic cultures as an *in vitro* model for investigating the dynamics of maturation processes.

Bursting activity in the isolated SOD1^{G93A} neonatal spinal cord

Our observations supported the presence of a greater proportion of glycine-GABA mixed synapses in organotypic and acute SOD1^{G93A} spinal cord slices compared to age-matched WT ones. Thus, we isolated (at P2–4 postnatal age) the entire spinal cord from WT and SOD1^{G93A} mice ($n = 7$ and 5, respectively) to further investigate whether MN outputs were influenced by the more prevalent GABA/glycine co-transmission. For this purpose, we measured spontaneous VR discharges. At early postnatal ages, spinal cords produced sporadic and irregular discharges in 61% of WT VRs and in 87% of SOD1^{G93A} VRs. In the mutant cords, such discharges were characterized by significantly longer depolarizing events (event duration: 2.8 ± 0.2 s WT and 6.3 ± 1.3 s SOD1^{G93A}, $P = 0.012$) (Fig. 5*A* and *B*). In particular, in the presence of GABA$_A$ receptor blockade, we studied MN outputs changes, potentially reflecting the faster kinetic of glycinergic synaptic events. In all WT and SOD1^{G93A} preparations, such MN outputs were transformed in robust synchronous bursts in the presence of a GABA$_A$ receptor blocker (SR-95531) used to isolate the glycinergic contribution (Fig. 5*C*). Notably, in SOD1^{G93A} spinal cords,

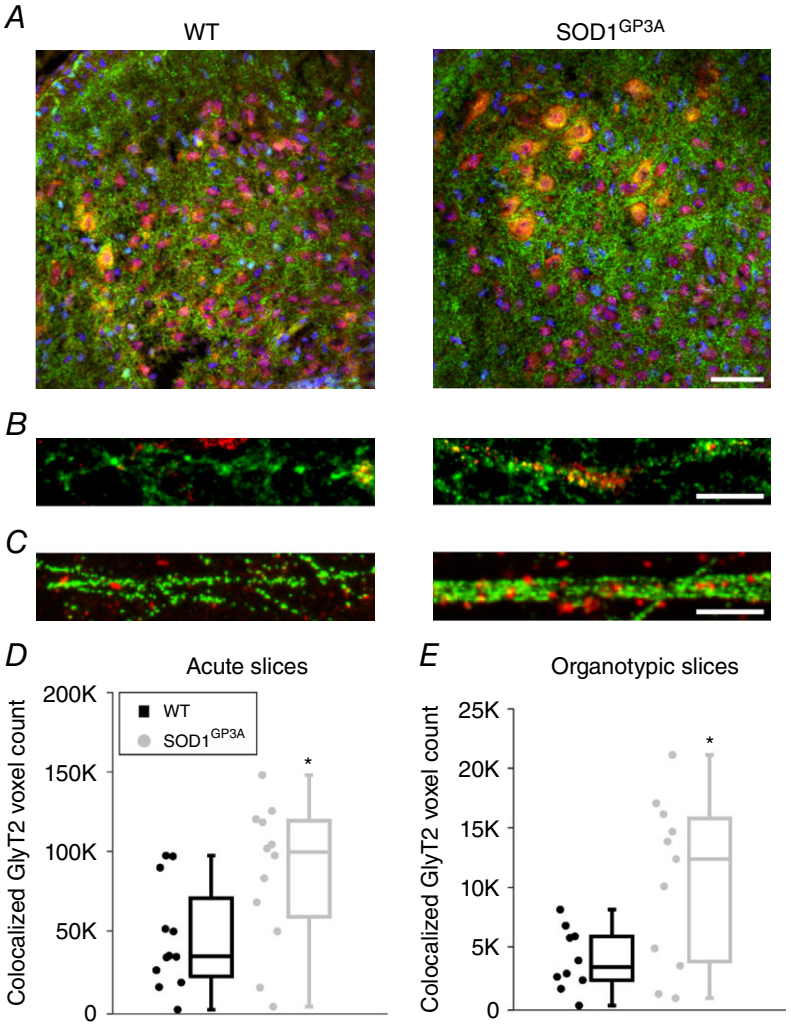

Figure 4. Co-localization of GlyT2 and GAD65 immunostaining in the WT and SOD1^{G93A} immature spinal cord
A, confocal images of the ventral horn of WT and SOD1^{G93A} acute spinal slices isolated from neonatal (P0) mice and stained for GlyT2 (green) and GAD65 (red). *B*, confocal high magnification of a region (from *A*) showing the appearance of GlyT2 (green) and GAD65 (red) clusters. Co-localization of GlyT2 (green) and GAD65 (red) clusters identify mixed synapses.
C, organotypic cultures: confocal high magnification of the ventral area of WT (left) and SOD1^{G93A} (right) cultured slices at 3 WIV, similar to the acute ones, co-localization of GlyT2 (green) and GAD65 (red) clusters identifies mixed synapses. *D* and *E*, box plots show that co-localized GlyT2 and GAD65 clusters are more common in SOD1^{G93A} (grey) spinal slices than in WT slices (black). This was seen both in acute slices (P0) (*D*, number of ROIs: 12 WT and 12 SOD1^{G93A}) and in cultured slices (3 WIV) (*E*, number of ROIs: 12 WT and 12 SOD1^{G93A}). Scale bar = 50 μm in (*A*), 10 μm in (*B* and *C*). $^*P < 0.05$.

the interbursts periods and burst durations were shorter, suggestive of an increased excitability (burst duration: 27.6 ± 3.5 s WT and 17.3 ± 1.9 s SOD1^{G93A}, $P = 0.0455$; interburst period: 64.6 ± 8.4 s WT and 39.2 ± 3.5 s SOD1^{G93A}, $P = 0.0284$) (Fig. 5*D*). These results further suggest that the tuning of inhibitory synapses is altered in SOD1^{G93A} spinal networks, which ultimately results in important changes in the whole spinal motor output.

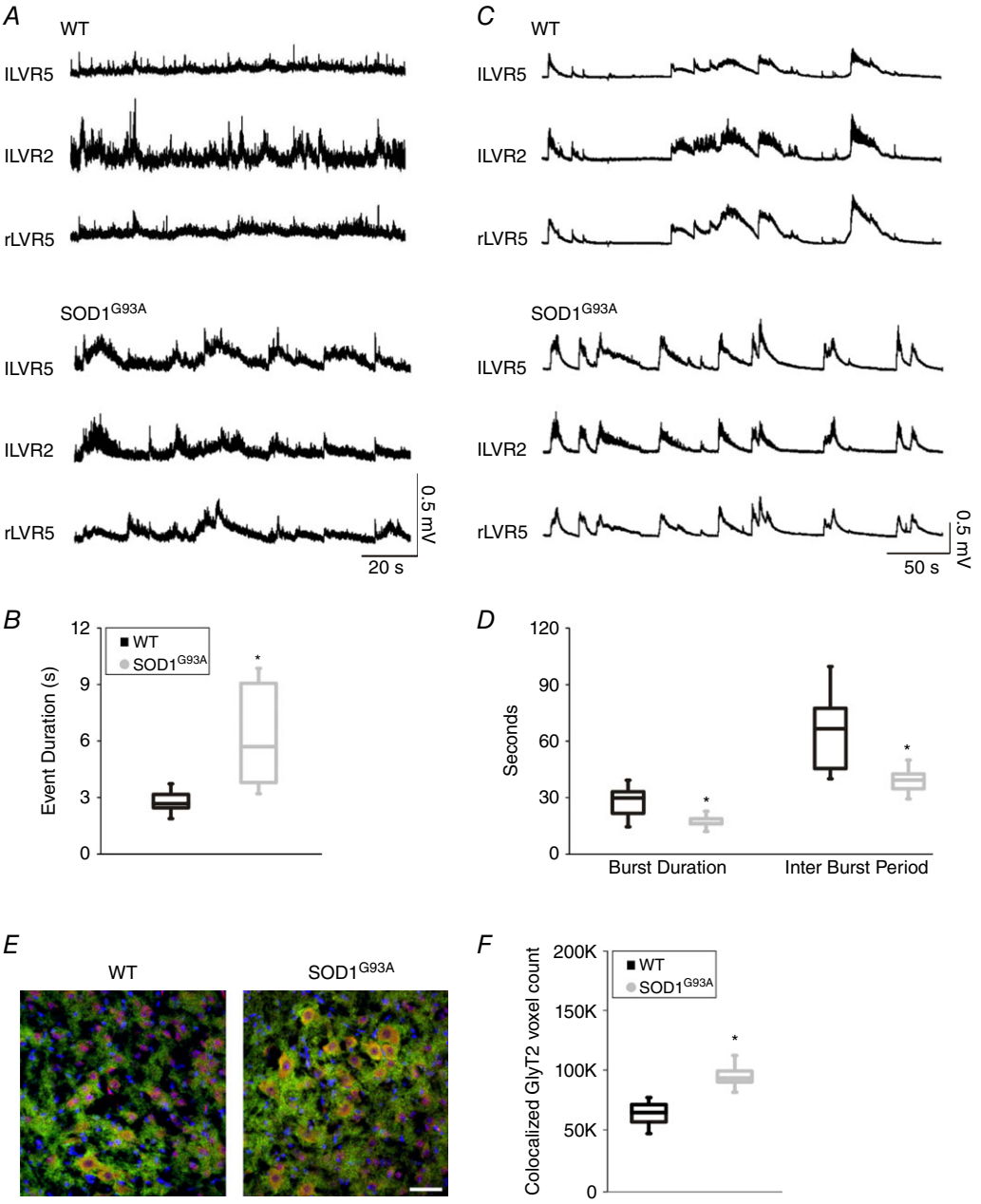

Figure 5. Motor output in WT and SOD1^{G93A} spinal cords isolated from P3 old mice
A, representative traces of spontaneous activity simultaneously recorded from left (l) and right (r) lumbar VR 5 (LVR5) and 2 (LVR2) in WT (top) and SOD1^{G93A} (bottom) spinal cords. *B*, box plots of event duration for WT (black, $n = 7$) and SOD1^{G93A} (grey, $n = 5$) spinal cord preparations. *C*, representative traces of VR activity recorded in the presence of SR-95531 in WT (top) and SOD1^{G93A} (bottom) spinal cords. *D*, box plots of burst duration and interburst period in WT (black, $n = 7$) and SOD1^{G93A} (grey, $n = 5$) mice. *E*, confocal images of ventral horn of WT (left) and SOD1^{G93A} (right) spinal cords (same preparations as recorded in *B*), the co-localization of GlyT2 (green) and GAD65 (red) clusters identify mixed synapses. *F*, box plots show the greater co-localization of GlyT2 and GAD65 clusters in SOD1^{G93A} spinal tissue (same preparations as recorded in *B*; number of ROIs: 5 WT and 5 SOD1^{G93A}). Scale bar = 50 μm. $^*P < 0.05$.

Discussion

Chang and Martin (2009, 2011) have shown that glycinergic inhibition of spinal MNs is impaired in the SOD1^{G93A} ALS animal model (Chang & Martin, 2009, 2011). In the present study, we used the organotypic cultures obtained from the same SOD1^{G93A} mice to investigate developmental changes in gly-PSCs in the pre-motor spinal network of presymptomatic ALS animals (Avossa *et al.* 2006). We recorded from interneurons to assess how changes in the pre-motor modulation of MN activity may contribute to the early pathogenesis of ALS. Characterizing ALS animal models throughout their development is important in an attempt to pinpoint the earliest alterations in synaptic input and neuronal excitability before the pathological process has progressed to denervation (Vinsant *et al.* 2013).

The present data show that, during *in vitro* development, the properties of gly-PSCs recorded from SOD1^{G93A} interneurons change in a pattern similar to that reported for WT gly-PSC in cultured and *ex-vivo* samples (Gao & Ziskind-Conhaim, 1995; Gao *et al.* 1998; Baccei & Fitzgerald, 2004). Thus, gly-PSCs become progressively more frequent, larger in amplitude and faster in their decay. However, we found that, at 3 WIV, an age in cultures equivalent to early postnatal days, gly-PSCs and mPSC from ALS model mice decay faster than those from WT neurons, resulting in a reduction in charge transfer in the range 20–35%.

To understand the reason for the observed difference in decay, we examined the main variables that change during development and might conceivably affect the kinetic properties of glycine receptors and therefore the gly-PSC time course. First, we excluded the possibility of differences in the intracellular chloride concentration that could affect gly-PSC kinetics (Pitt *et al.* 2008). Our measurements show that the Cl^- reversal potential was similar in the two cultures at matching *in vitro* ages. In both WT and transgenic cultures, the Cl^- reversal potential differed from the predicted theoretical value. In our recording conditions, it is not possible to distinguish between an impaired pipette/cell solution-exchange as a result of maturation-dependent changes in neuronal morphology or a real shift in the internal chloride concentration as a result of improved extrusion (DeFazio et al 2000; Ostroumov *et al.* 2011). However, the detected shifts are similar in both WT and SOD1^{G93A} interneurones dialysed with a 24 mM Cl^- intracellular pipette solution.

Another well-documented process that changes glycinergic inhibition in the developing CNS is the switch from the expression of $\alpha 2$ homomeric channels to that of the adult synaptic $\alpha 1\beta$ heteromeric GlyR (Takahashi *et al.* 1992, Singer & Berger, 1999). Heteromeric $\alpha 1\beta$ receptors have a faster deactivation (Mangin et al. 2003; Pitt *et al.* 2008; Krashia *et al.* 2011), which results in a faster decaying synaptic current (Zhang *et al.* 2015). Heteromeric glycine receptors have a smaller conductance than homomeric channels (Bormann *et al.* 1993) and thus we recorded single channel activity from outside-out patches to establish whether the time course of appearance of heteromeric isoforms differed at 2 and 3 WIV in WT and SOD1^{G93A} mice. At 2 WIV, the gradual shift towards the more mature receptor type appeared to be more pronounced in WT patches, although the proportion of heteromeric *vs.* homomeric patches was very similar at the 3 WIV stage of development. These data suggest that the faster decay of SOD1^{G93A} gly-PSC cannot be the result of an earlier or more complete switch to heteromeric channels. However, we must interpret these findings with caution, given that outside-out patches are likely to contain mostly extrasynaptic receptors and that, by its very nature, single channel recording is not an accurate way of estimating the proportion of one type of channel *vs.* the other.

We turned our attention to presynaptic processes that may affect synaptic time course. The timing of glycinergic inhibition is known to be regulated by the extent of release synchronization, which can make the PSC longer than the channel deactivation (Balakrishnan *et al.* 2009). Differences in release synchronization between WT and SOD1^{G93A} synapses probably do not explain our data because, in SOD1^{G93A} neurons, the decay of gly-PSCs is also faster for unitary synaptic events (mPSCs).

This leaves the possibility that our findings can be explained by differences in GABA co-release; namely, that this persists longer in SOD1^{G93A} cultures. At auditory synapses, GABA co-release makes the PSC faster than the channel deactivation by the partial agonist action of GABA on glycine receptors (Lu *et al.* 2008). GABA/glycine co-expression is developmentally regulated in the spinal cord. Its extent decreases with development (Allain *et al.* 2006; Sibilla & Ballerini, 2009) and can be affected by the pattern of activity at the synapse (Nerlich *et al.* 2014). After depletion of GABA presynaptic content by TBOA applications (Lu *et al.* 2008), we observed that SOD1^{G93A} gly-PSCs were no longer significantly different compared to WT in terms of decay time.

Our hypothesis was further strengthened by the detection of greater proportion of GABA-glycine mixed synapses (Dumoulin *et al.* 2001; Mackie *et al.* 2003; Dugué *et al.* 2005) in transgenic tissue *vs.* WT, both in cultured and in *ex vivo* spinal preparations. These results suggest that the faster decay of gly-PSC in ALS model mice is largely a result of the longer persistence of GABA co-release.

In developing spinal circuits, during the emergence of organized motor behaviours, the fine-tuning and refinement of inhibitory neurotransmission, including the regulation of GABA/glycine co-release, comprise a complex, region-specific phenomenon (Jonas et al 1998; Keller et al 2001; Gonzalez-Forero & Alvarez, 2005; Sibilla & Ballerini, 2009). In the present study, we report

for the first time that, at ages corresponding to the higher detection of GABA at glycinergic synapses in SOD1^{G93A} ventral horn, the emerging motor outputs show more prolonged spontaneous bursting in SOD1^{G93A} VR-recordings. This finding is consistent with the proposal of a delayed maturation of GABAergic/glycinergic inhibitory interneuronal connections (Whelan, 2003). In addition, the reduction of the gly-PSC duration as a result of the persistence of GABA/glycine co-release in SOD1^{G93A} spinal cord is confirmed by increased VR bursting, a clear symptom of increased MN pool excitability (Bracci *et al.* 1997; Ballerini *et al.* 1999), when motor outputs are recorded in the presence of a $GABA_A$ receptor antagonist.

In conclusion, the main finding of the present study is that SOD1^{G93A} networks display abnormal premotor network maturation long before the appearance of any symptom and in the absence of early sign of degeneration (Avossa *et al.* 2006). The alteration in glycinergic inhibition might involve spinal ventral interneurons, and not only MNs as suggested previously (Chang & Martin, 2009, 2011). The changes in operation of gly-PSCs may impair the optimal development of MN outputs: understanding how this occurs may provide clearer insights into the underlying threat to MNs viability in ALS patients.

References

Aguayo LG, van Zundert B, Tapia JC, Carrasco MA & Alvarez FJ (2004). Changes on the properties of glycine receptors during neuronal development. *Brain Res Rev* **47**, 33–45.

Allain AE, Baïri A, Meyrand P & Branchereau P (2006). Expression of the glycinergic system during the course of embryonic development in the mouse spinal cord and its co-localization with GABA immunoreactivity. *J Comp Neurol* **496**, 832–846.

Avossa D, Rosato-Siri MD, Mazzarol F & Ballerini L (2003). Spinal circuits formation: a study of developmentally regulated markers in organotypic cultures of embryonic mouse spinal cord. *Neuroscience* **122**, 391–405.

Avossa D, Grandolfo M, Mazzarol F, Zatta M & Ballerini L (2006). Early signs of motoneuron vulnerability in a disease model system: characterization of transverse slice cultures of spinal cord isolated from embryonic ALS mice. *Neuroscience* **138**, 1179–1194.

Baccei ML & Fitzgerald M (2004). Development of GABAergic and glycinergic transmission in the neonatal rat dorsal horn. *J Neurosci* **24**, 4749–4757.

Balakrishnan V, Kuo SP, Roberts PD & Trussell LO (2009). Slow glycinergic transmission mediated by transmitter pooling. *Nature Neurosci* **12**, 286–294

Ballerini L & Galante M (1998). Network bursting by organotypic spinal slice cultures in the presence of bicuculline and/or strychnine is developmentally regulated. *Eur J Neurosci* **10**, 2871–2879.

Ballerini L, Galante M, Grandolfo M & Nistri A (1999). Generation of rhythmic patterns of activity by ventral interneurons in rat organotypic spinal slice culture. *J Physiol* **517**, 459–475.

Bracci E, Ballerini L & Nistri A (1996). Spontaneous rhythmic bursts induced by pharmacological block of inhibition in lumbar motoneurons of the neonatal rat spinal cord. *J Neurophysiol* **75**, 640–647.

Bracci E, Beato M & Nistri A. (1997). Afferent inputs modulate the activity of a rhythmic burst generator in the rat disinhibited spinal cord in vitro. *J Neurophysiol.* **77**, 3157–3167.

Beato M & Nistri A (1999). Interaction between disinhibited bursting and fictive locomotor patterns in the rat isolated spinal cord. *J Neurophysiol* **82**, 2029–2038.

Beato M & Sivilotti LG (2007). Single-channel properties of glycine receptors of juvenile rat spinal motoneurones in vitro. *J Physiol* **580**, 497–506.

Ben-Ari Y (2008). Neuro-archaeology: pre-symptomatic architecture and signature of neurological disorders. *Trends Neurosci* **31**, 626–636.

Bormann J, Rundstrom N, Betz H & Langosch D (1993). Residues within transmembrane segment M2 determine chloride conductance of glycine receptor homo- and hetero-oligomers. *EMBO J* **12**, 3729–3737.

Chang Q & Martin LJ (2009). Glycinergic innervation of motoneurons is deficient in amyotrophic lateral sclerosis mice: a quantitative confocal analysis. *Am J Pathol* **174**, 574–585.

Chang Q & Martin LJ (2011). Glycine receptor channels in spinal motoneurons are abnormal in a transgenic mouse model of amyotrophic lateral sclerosis. *J Neurosci* **31**, 2815–2827.

Cirulli ET, Lasseigne BN, Petrovski S, Sapp PC, Dion PA, *et al* (2015). Exome sequencing in amyotrophic lateral sclerosis identifies risk genes and pathways. *Science* **347**, 1436–41

Clements JD & Bekkers JM (1997). Detection of spontaneous synaptic events with an optimally scaled template. *Biophys J* **73**, 220–229.

Copray JC, Jaarsma D, Kust BM, Bruggeman RW, Mantingh I, Brouwer N & Boddeke HW. (2003). Expression of the low affinity neurotrophin receptor p75 in spinal motoneurons in a transgenic mouse model for amyotrophic lateral sclerosis. *Neuroscience* **116**, 685–694.

DeFazio RA, Keros S, Quick MW & Hablitz JJ. (2000). Potassium-coupled chloride cotransport controls intracellular chloride in rat neocortical pyramidal neurons. *J Neurosci* **20**, 8069–8076.

Dugué GP, Bumoulin A, Triller A & Dieudonné S (2005). Target-dependent use of coreleased inhibitory transmitters at central synapses. *J Neurosci* **25**, 6490–6498.

Dumoulin A, Triller A & Dieudonné S (2001). IPSC kinetics at identified GABAergic and mixed GABAergic and glycinergic synapses onto cerebellar golgi cells. *J Neurosci* **21**, 6045–6057.

Furlan F, Guasti L, Avossa D, Becchetti A, Cilia E, Ballerini L & Arcangeli A (2005). Interneurons transiently express the ERG K^+ channels during development of mouse spinal networks in vitro. *Neuroscience* **135**, 1179–1192.

Furlan F, Taccola G, Grandolfo M, Guasti L, Arcangeli A, Nistri A & Ballerini L (2007). ERG conductance expression modulates the excitability of ventral horn GABAergic interneurons that control rhythmic oscillations in the developing mouse spinal cord. *J Neurosci* **27**, 919–928.

Galante M, Nistri A & Ballerini L (2000). Opposite changes in synaptic activity of organotypic rat spinal cord cultures after chronic block of AMPA/kainate or glycine and $GABA_A$ receptors. *J Physiol* **523**, 639–651.

Gao BX & Ziskind-Conhaim L (1995). Development of glycine- and GABA-gated currents in rat spinal motoneurons. *J Neurophysiol* **74**, 113–121.

Gao BX, Cheng G & Ziskind-Conhaim L (1998). Development of spontaneous synaptic transmission in the rat spinal cord. *Neurophysiology* **79**, 2277–2287.

González-Forero D & Alvarez FJ. (2005). Differential postnatal maturation of $GABA_A$, glycine receptor, and mixed synaptic currents in Renshaw cells and ventral spinal interneurons. *J Neurosci* **25**, 2010–2023.

Gurney ME, Pu H, Chiu AY, Dal Canto MC, Polchow CY, Alexander DD, Caliendo J, Hentati A, Kwon YW, Deng HX, Chen W, Zhai P, Sufit RL & Siddique T (1994). Motor neuron degeneration in mice that express a human Cu,Zn superoxide dismutase mutation. *Science* **264**, 1772–1775.

Holasek SS, Wengenack TM, Kandimalla KK, Montano C, Gregor DM, Curran GL & Poduslo JF (2005). Activation of the stress-activated MAP kinase, p38, but not JNK in cortical motor neurons during early presymptomatic stages of amyotrophic lateral sclerosis in transgenic mice. *Brain Res* **1045**, 185−198.

Keller AF, Coull JA, Chery N, Poisbeau P & De Koninck Y. (2001). Region-specific developmental specialization of GABA-glycine cosynapses in laminas I-II of the rat spinal dorsal horn. *J Neurosci* **21**, 7871–80.

Krashia P, Lape R, Lodesani F, Colquhoun D & Sivilotti LG (2011). The long activations of α2 glycine channels can be described by a mechanism with reaction intermediates ('flip'). *J Gen Physiol* **137**, 197–216.

Jonas P, Bischofberger J & Sandkühler J. (1998). Corelease of two fast neurotransmitters at a central synapse. *Science* **281**, 419–424.

Ling SC, Polymenidou M & Cleveland DW (2013). Converging mechanisms in ALS and FTD: disrupted RNA and protein homeostasis. *Neuron* **79**, 416–438.

Lynch JW (2009). Native glycine receptor subtypes and their physiological roles. *Neuropharmacology* **56**, 303–309.

Lu T, Rubio ME & Trussell LO (2008). Glycinergic transmission shaped by corelease of GABA in a mammalian auditory synapse. *Neuron* **57**, 524–535.

Mackie M, Hughes DI, Maxwell DJ, Tillakaratne NJ & Todd AJ (2003). Distribution and colocalisation of glutamate decarboxylase isoforms in the rat spinal cord. *Neurosci* **119**, 461–472.

Malosio ML, Marqueze-Pouey B, Kuhse J & Betz H (1991). Widespread expression of glycine receptor subunit mRNAs in the adult and developing rat brain. *EMBO J* **10**, 2401–2409.

Mangin JM, Baloul M, Prado De Carvalho L, Rogister B, Rigo JM & Legendre P (2003). Kinetic properties of the alpha2 homo-oligomeric glycine receptor impairs a proper synaptic functioning. *J Physiol* **553**, 369–386.

Martin LJ & Chang Q (2012). Inhibitory synaptic regulation of motoneurons: a new target of disease mechanisms in amyotrophic lateral sclerosis. *Mol Neurobiol* **45**, 30–42.

Mathews GC & Diamond JS (2003). Neuronal glutamate uptake contributes to GABA synthesis and inhibitory synaptic strength. *J Neurosci* **23**, 2040–2048.

McGoldrick P, Joyce PI, Fisher EM & Greensmith L (2013). Rodent models of amyotrophic lateral sclerosis. *Biochim Biophys Acta* **1832**, 1421–1436.

Nerlich J, Kuenzel T, Keine C, Korenic A, Rübsamen R & Milenkovic I (2014). Dynamic fidelity control to the central auditory system: synergistic glycine/GABAergic inhibition in the cochlear nucleus. *J Neurosci* **34**, 11604–11620.

Nigro A, Menon R, Bergamaschi A, Clovis YM, Baldi A, Ehrmann M, Comi G, De Pietri Tonelli D, Farina C, Martino G & Muzio L (2012). MiR-30e and miR-181d control Radial Glia cell proliferation via HtrA1 modulation. *Cell Death Dis* **3**, e360.

Ostroumov A, Simonetti M & Nistri A. (2011). Cystic fibrosis transmembrane conductance regulator modulates synaptic chloride homeostasis in motoneurons of the rat spinal cord during neonatal development. *Dev Neurobiol* **71**, 253–268.

Pitt SJ, Sivilotti LG & Beato M (2008). High intracellular chloride slows the decay of glycinergic currents. *J Neurosci* **28**, 11454–11467.

Rao SD, Yin HZ & Weiss JH (2003). Disruption of glial glutamate transport by reactive oxygen species produced in motor neurons. *J Neurosci* **23**, 2627−2633.

Robberecht W & Philips T (2013). The changing scene of amyotrophic lateral sclerosis. *Nat Rev Neurosci* **14**, 248–264.

Rosato-Siri MD, Zoccolan D, Furlan F & Ballerini L (2004). Interneurone bursts are spontaneously associated with muscle contractions only during early phases of mouse spinal network development: a study in organotypic cultures. *Eur J Neurosci* **20**, 2697–2710.

Rothstein JD (2003). Of mice and men: reconciling preclinical ALS mouse studies and human clinical trials. *Ann Neurol* **53**, 423–426.

Rothstein JD (2009). Current hypotheses for the underlying biology of amyotrophic lateral sclerosis. *Ann Neurol* **65** Suppl 1, S3–S9.

Shimamoto K, LeBrun B, Yasuda-Kamatani Y, Sakaitani M, Shigeri Y, Yumoto N & Nakajima T (1998). DL-threo-β-benzyloxyaspartate, a potent blocker of excitatory amino acid transporters. *Mol Pharmacol* **53**, 195–201.

Schutz B (2005). Imbalanced excitatory to inhibitory synaptic input precedes motor neuron degeneration in an animal model of amyotrophic lateral sclerosis. *Neurobiol Dis* **20**, 131–40.

Sibilla S & Ballerini L (2009). GABAergic and glycinergic interneuron expression during spinal cord development: dynamic interplay between inhibition and excitation in the control of ventral network outputs. *Progress Neurobiol* **89**, 46–60.

Singer JH, Talley EM, Bayliss DA & Berger AJ (1998). Development of glycinergic synaptic transmission of rat brain stem motoneurons. *J Neurophysiol* **80**, 2608–2620.

Singer JH & Berger AJ (1999). Contribution of single-channel properties to the time course and amplitude variance of quantal glycine currents recorded in rat motoneurons. *J Neurophysiol* **81**, 1608–1616.

Streit J, Spenger C & Lüscher HR (1991). An organotypic spinal cord – dorsal root ganglion – skeletal muscle coculture of embryonic rat. II. Functional evidence for the formation of spinal reflex arcs in vitro. *Eur J Neurosci* **3**, 1054–1068.

Taccola G, Margaryan G, Mladinic M & Nistri A (2008). Kainate and metabolic perturbation mimicking spinal injury differentially contribute to early damage of locomotor networks in the *in vitro* neonatal rat spinal cord. *Neurosci* **155**, 538–555.

Takahashi T, Momiyama A, Hirai K, Hishinuma F & Akagi H (1992). Functional correlation of fetal and adult forms of glycine receptors with developmental changes in inhibitory synaptic receptor channels. *Neuron* **9**, 1155–1161.

Turner BJ & Talbot K (2008). Transgenics, toxicity and therapeutics in rodent models of mutant SOD1-mediated familial ALS. *Prog Neurobiol* **85**, 94–134.

Veeraraghavan P & Nistri A (2015). Modulatory effects by CB1 receptors on rat spinal locomotor networks after sustained application of agonists or anatagonists. *Neuroscience* **303**, 16–33.

Vinsant S, Mansfield C, Jimenez-Moreno R, Del Gaizo Moore V, Yoshikawa M, Hampton TG, Prevette D, Caress J, Oppenheim RW & Milligan C (2013). Characterization of early pathogenesis in the SOD1(G93A) mouse model of ALS: part I, background and methods. *Brain Behav* **3**, 335–350.

Whelan PJ. (2003). Developmental aspects of spinal locomotor function: insights from using the in vitro mouse spinal cord preparation. *J Physiol* **553**, 695–706.

Zhang Y, Dixon CL, Keramidas A & Lynch JW (2015). Functional reconstitution of glycinergic synapses incorporating defined glycine receptor subunit combinations. *Neuropharmacology* **89**, 391–397.

Additional information

Competing interests

The authors declare that they have no competing interests.

Author contributions

MM and VR performed synaptic electrophysiology and all the experimental analysis on slice cultures. MM and PV performed spinal cord VR recordings. MM and JL designed and performed the immunofluorescence, confocal microscopy and image analysis on acute and cultured spinal slices. GC performed and analysed the single channel electrophysiology. CR and LM performed the isolation of acute slices and processing for histology. LS designed the single channel experiments and also drafted and revised the MS critically for important intellectual content. LB conceived the study, designed the experiments, designed and contributed to the analysis of data, and wrote the manuscript. All authors discussed the results and approved the final version of the manuscript and agree to be accountable for all aspects of the work in ensuring that questions related to the accuracy or integrity of any part of the work are appropriately investigated and resolved. All persons designated as authors qualify for authorship, and all those who qualify for authorship are listed.

Funding

We acknowledge financial support from the NEUROSCAFFOLDS-FP7-NMP-604263 and PRIN-MIUR n. 2012MYESZW. G. Cellot was supported by the Fondazione Alberto and Kathleen Casali, Trieste, Italy.

Acknowledgements

We are especially grateful to Professor Andrea Nistri for his helpful comments and for supervising the entire spinal cord experiments and to Dr Micaela Grandolfo for supervising the immune staining and its quantification.